Available online at www.sciencedirect.com
ScienceDirect
Trans. Nonferrous Met. Soc. China 24(2014) 3170−3180
Transactions of Nonferrous Metals Society of China
www.tnmsc.cn

In-situ formation characteristic, tribological characterization and anti-corrosion properties of quaternary composites films

Ojo Sunday Isaac FAYOMI, Abimbola Patricia Idowu POPOOLA

Department of Chemical, Metallurgical and Materials Engineering,
Tshwane University of Technology, P.M.B. X680, Pretoria, South Africa

Received 16 November 2013; accepted 23 May 2014

Abstract: Improvements of wear and corrosion properties are essential characteristic in engineering application. A study was made on the structure, electro-oxidation and properties of fabricated Zn−Al−SnO_2−TiO_2 (Zn−Al−Sn−Ti) thin films using electrodeposition technique from chloride bath. The microstructural studies were performed by scanning electron microscopy with attached energy dispersive spectrometer (SEM−EDS), optical microscopy (OPM) and X-ray diffractogram (XRD). The electrochemical oxidation and erosion behavior in 3.65% NaCl medium were studied by potentiodynamic polarization technique and characterized by atomic force microscopy (AFM). The hardness and wear behavior of the electrodeposited film were performed by high diamond dura scan microhardness tester and CERT UMT-2 reciprocating sliding machine. It was found that a successful co-deposition of composite and particle were attained. Homogeneous imbedded grain structure distribution and fine refinement of crystal with improved micromechanical behavior was achieved. The corrosion resistance, hardness and wear stability resistance of the fabricated quaternary films improved significantly in all varied process parameter.

Key words: co-deposition; microstructural evolution; anti-corrosion property; composite materials

1 Introduction

Over decade, thin films electrodeposition has been widely applied in most engineering industries from automobile, photo-electronics, aerospace and marine to mention [1−6]. Much attention has been paid to binary admixed metal matrix alloy, lately especially with Zn particles [5−12]. But with higher pH value in acidic medium and high temperature range, corrosion and wear resistance properties from the binary fabricated processing are limited in service performance [1,13−20].

In view of this, codeposition reinforced metal matrix composite electrodeposition has been used to enhance and provide specific desirable properties [21−26]. Metal−ceramic matrixes, such as TiO_2 [1,16], SiO_2 [11,25], ZrO_2 [14], Cr_2O_3 [10,24], Al_2O_3 and ZnO [14,17,18], have been tested to provide enhanced strengthening properties and good surface modified behavior.

However, in an attempt to further provide continuous mechanical and morphological characteristics, replacement of binary bath formulation is necessary in relation to bath control parameters. Quaternary coatings are very limited [9−11]. The individual difference in microstructure and adhesion behavior of Al_2O_3 [9,20,21], TiO_2 [16,18,27] and SnO_2 [28,29] is known to possess high hardness, thermal stability and improved structural crystal. The quaternary fabricated formulation of this blend in single bath could guarantee a secondary phase and crystal growth. In the present study, Zn−Al−SnO_2−TiO_2 (Zn−Al−Sn−Ti) composite particulates were processed and fabricated from chloride electrolyte. The structural properties, mechanical stability and tribological characteristics of the coatings were investigated.

2 Experimental

2.1 Electrodeposition process

The chemicals used were of AR grade. Distilled water was used for the preparation of admixed bath solutions. The coating of Zn−Al−Sn−Ti in chloride bath was achieved through a designed cell consisting of two anode electrodes and a cathode electrode as described in Fig. 1.

Corresponding author: Ojo Sunday Isaac FAYOMI; Tel: +234-8036886783; +27-12-382-3513; E-mail: ojosundayfayomi3@gmail.com; popoolaapi@tut.ac.za

DOI: 10.1016/S1003-6326(14)63457-9

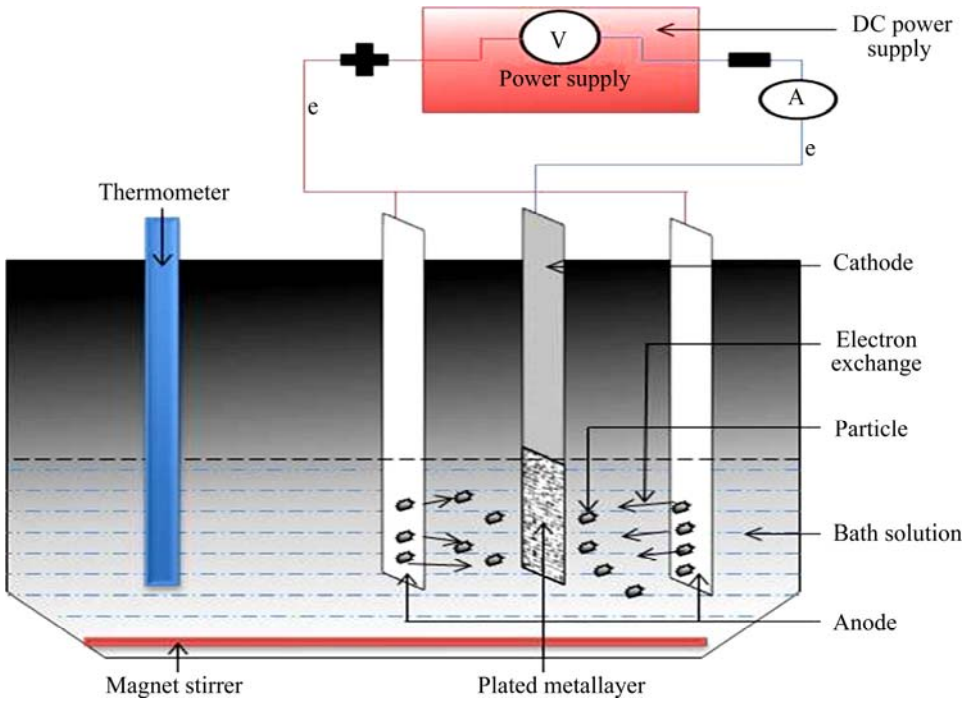

Fig. 1 Schematic diagram of electrodeposited cell

The dimensions of the mild steel sheet (substrate) used were 40 mm×20 mm×1 mm and zinc sheet of 50 mm×30 mm×3 mm was prepared as anode. The chemical composition of the mild steel substrate is shown in Table 1.

Table 1 Chemical composition of mild steel used (mass fraction, %)

C	Mn	Si	P	S	Al	Ni	Fe
0.15	0.45	0.18	0.01	0.031	0.005	0.008	Bal.

The zinc chemical composition was 99.99%. Prior to the plating, the mild steel specimens were polished mechanically, degreased and rinsed with water as described in Refs. [7,20]. In the pre-plating process, the surface preparation was done on a polishing machine with different grades of emery paper in order of 60, 120, 400, 800 and 1600 μm grades. Water was added intermittently so as to cool down the metal samples. During the grinding operation, the metal samples were rotated at an angle of 90° or 180° at intervals to erase previous marks which arose due to the initial grinding. The pickling of the samples was done in diluted HCl acid solution to remove all organic contaminants and oxides, followed by electrolytic degreasing. The prepared cathode and anodes were connected to the DC power supply through a rectifier at a varying voltage of 0.3−0.5 V with varying applied current density of 2 A/cm^2 for 20 min. The bath composition of the coated pattern is illustrated in Tables 2 and 3.

2.2 Structural characterization

The surface morphology studies of the deposits were observed by a scanning electron microscope (SEM) equipped with an energy dispersive spectroscope (EDS) (model: VEGA 3 TESCAN). Atomic force microscope was used to quantify the surface topography and morphology of the plated test specimens. The phase change of the coatings was determined by X-ray diffractogram (XRD).

Wear analysis was carried out by a CERT UMT−2 multi-functional sliding tester with design diagram shown in Fig. 2. The reciprocating sliding tests were carried out with a load of 5 N, constant speed of 5 mm/s, displacement amplitude of 2 mm in 20 min. The wear scars structural evolutions were examined with a high optic Nikon optical microscope (OPM).

The Vickers microhardness of the coating was examined by the dwell indentation technique for 15 s across the interface with a summarized average using dura scan inventor-EMCOTEST.

2.3 Electrochemical studies

The electrochemical resistance study was evaluated using linear potentiodynamic polarization test on the deposited samples. Measurements were systematically evaluated using an Autolab potentiostat (PGSTAT101 computer controlled) with the general purpose electrochemical software (NOVA) package version. Measurements were made at room temperature using 3.65% NaCl solution. The solution for this study was

Table 2 Summarized data of plated samples for Zn−Al−SnO_2−TiO_2 from chloride bath

ρ(Zn)/(g·L^{-1})	ρ(Al)/(g·L^{-1})	ρ(KCl)/(g·L^{-1})	ρ(boric acid)/(g·L^{-1})	m(SnO_2)/g	m(TiO_2)/g
75	30	50	10	7,13	7,13
ρ(ZnCl)/(g·L^{-1})	pH	Voltage/V	Time/min	Temperature/°C	Current density/(A·cm^{-2})
75	4.8	0.3, 0.5	20	40	2

Table 3 Itinerary bath composition of quaternary Zn−Al−Sn−Ti−S alloy co-deposition

Sample No.	Material	Time of deposition/min	Potential/V	Current density/ (A·cm^{-2})
1	Zn−Al−7Sn−Ti−0.3V−Cl	20	0.3	2
2	Zn−Al−7Sn−Ti−0.5V−Cl	20	0.5	2
3	Zn−Al−13Sn−Ti−0.3V−Cl	20	0.3	2
4	Zn−Al−13Sn−Ti−0.5V−Cl	20	0.5	2

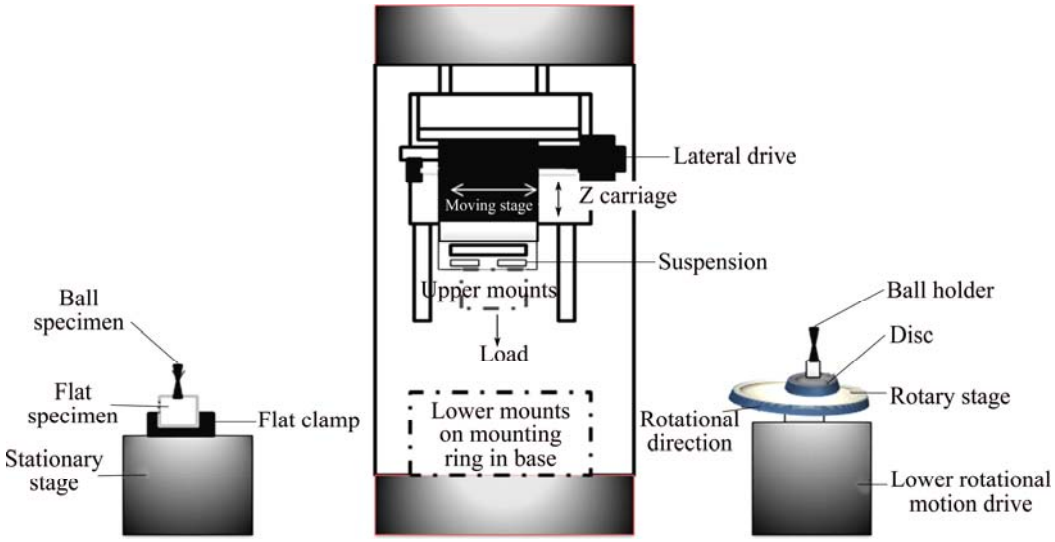

Fig. 2 Schematic view of reciprocating sliding friction CERT UMT−2 test system

prepared from analytical grade reagents and distilled water. An electrochemical cell consisting of working electrode (samples), graphite rods as the counter electrodes and a silver/silver chloride electrode as the reference electrode (SCE) in 3 mol/L KCl from −1.51 V to 1.5 V scanned potential at a scan rate of 0.0012 V was used for the potentiodynamic examination.

3 Results and discussion

3.1 SEM/EDS characterization of materials

Figure 3 illustrates the SEM images of as-received sample before coating. The surface features of the as-received sample show iron and carbon as a major constituent from EDS spectra. Figures 4 and 5 respectively show SEM images and EDS results of the deposited quaternary alloy at different induced additives concentrations under varied applied potentials as listed in Table 3. From all processed coatings, the distribution of the coating is unique and the average content of the element is also visible through the EDS studies. The effects of composite induced particulates are obvious as the small crystal was formed through the interface of the coated metal.

Although, it is a known and attested fact that in deposition, bath mediums with micro size composite in figment and conditioning will possibly produce solid materials with improved morphological properties for advanced processing [7,15]. In fact, the adsorption of the composite oxide particulates could have a great effect on the strengthening behavior of the coated metal and formation of the subsequent adhesion as shown in the nature of crystal growth illustrated in Fig. 4.

According to Refs. [20,26], deposit composition is a factor for structural evolution and better adhesion characteristics. The small grains solid dispatched observed in Figs. 4 and 5 at all applied potentials are attributed to the induced effect of the control process parameters. An increase or decrease in applied potential or current, sometimes regulates the uniform arrangement of crystals and hence results in the fine grained deposits exhibiting coalesced crystallites depending on process

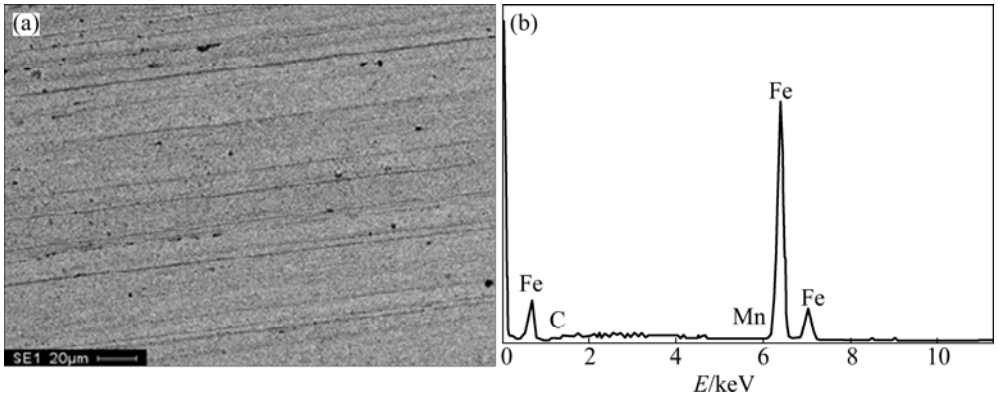

Fig. 3 SEM image (a) and EDS result (b) of as-received mild steel

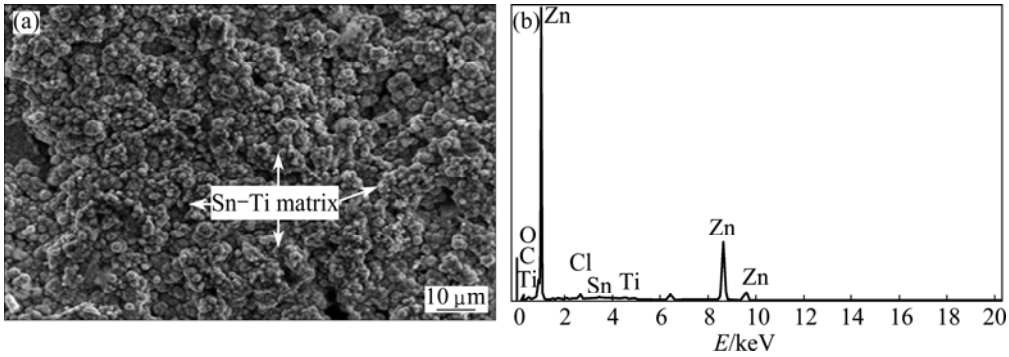

Fig. 4 SEM image (a) and EDS result (b) of Zn−Al−7Sn−Ti−0.3V chloride deposited sample

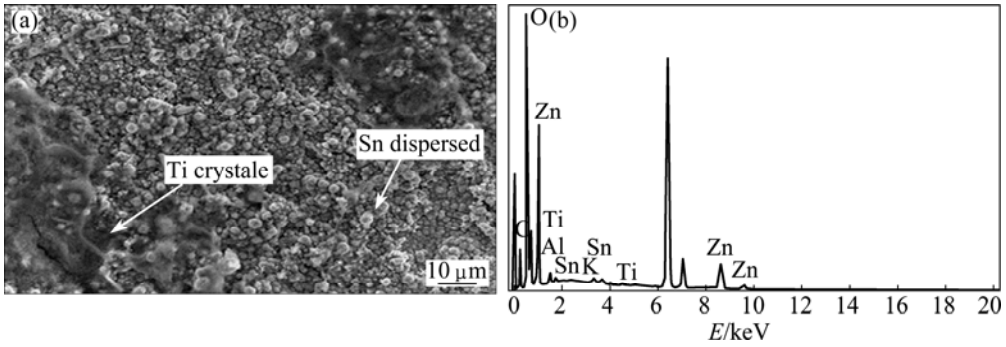

Fig. 5 SEM image (a) and EDS result (b) of Zn−Al−13Sn−Ti−0.5V chloride deposited sample

variable [12,30].

Both Zn−Al−7Sn−Ti−0.3V−Cl and Zn−Al−13Sn−Ti−0.5V−Cl produced a homogenous, smooth and more stable modification. The difference in stability could not be seen virtually under both subjected conditions. This implies that effects of electron transfer rate and throwing power are function of applied potential or current and this assists the possible modification of crystal growth and further penetration of blocking effect of vacancies with the help of particle induced within the cathode site. The individual regularity of the dispatch homogeneous distribution that the particles possess is indicated with the help of EDS with peak variance of major elemental constituent.

Figure 6 shows the optical micrographs of the deposited samples with adhered structure and uniform crystal blooming at the interface of Zn−Al−7Sn−Ti−0.3V and better texture as a result of fabricated condition. There is little dispatch in the case of 13 g/L SnO_2 in Zn−Al−13Sn−Ti−0.5V composite coating from microstructural point of view.

3.2 Atomic force micrograph

Figures 7 and 8 show 3D atomic force micrographs (AFM) of co-deposited structures under different conditions. For the sample with Zn−Al−7Sn−Ti−0.3V

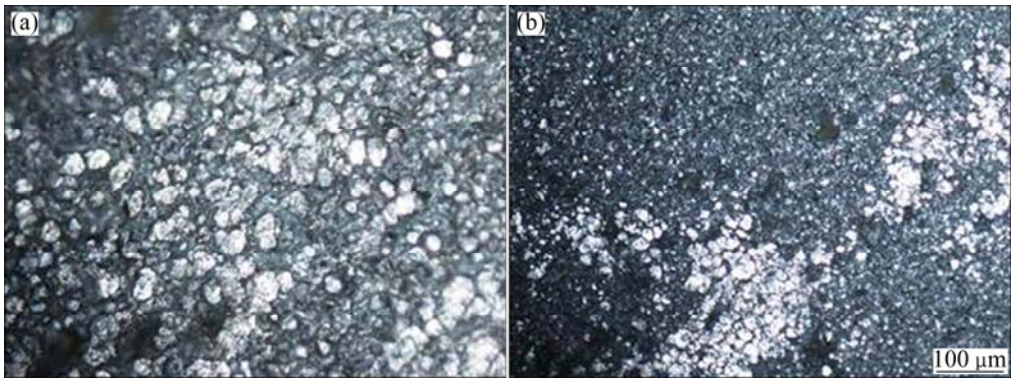

Fig. 6 Optical micrographs of Zn−Al−7Sn−Ti−0.3V (a) and Zn−Al−13Sn−Ti−0.5V (b) chloride deposited sample

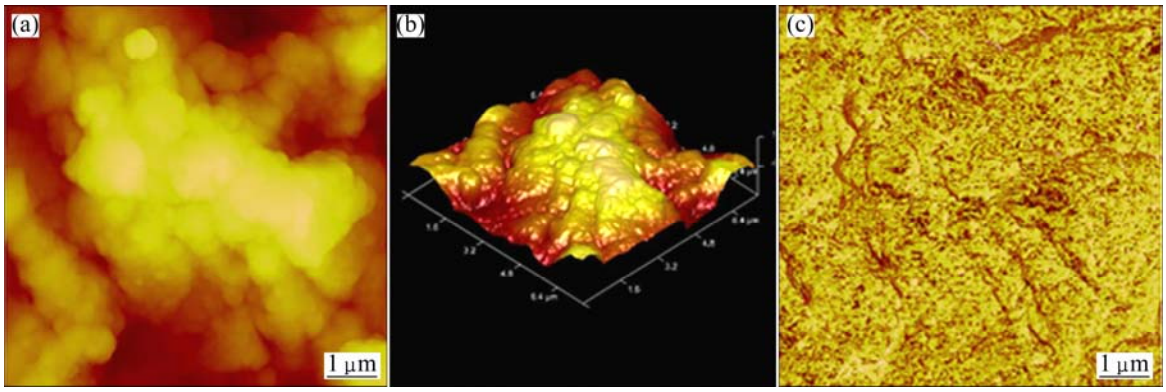

Fig. 7 AFM images of Zn−Al−7Sn−Ti−0.3V−Cl film obtained for 2D image (a), 3D relief image (b) and roughness analysis (c)

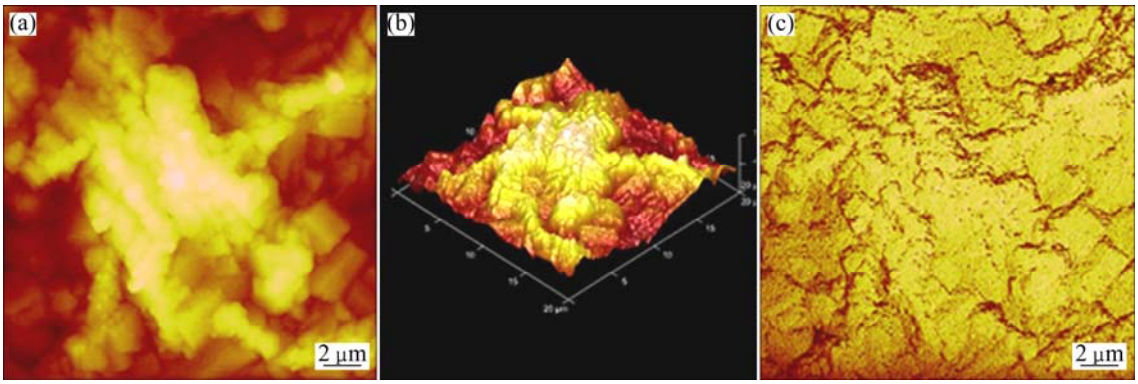

Fig. 8 AFM images of Zn−Al−13Sn−Ti−0.3V−Cl film obtained for 2D image (a), 3D relief image (b) and roughness analysis (c)

matrix in bath control of 7 g/L SnO_2, the topography and distribution of the deposited films are stable. Grain size and crystal growth uniformity were obtained (see Fig. 7). The distribution of the particulates from the topographic view was not regular when SnO_2 increased to 13 g/L as compared with 7 g/L SnO_2. It is evident that dispatched 7 g/L SnO_2 particles in bath seem moderately saturated, which provides good refinement in grain size and better microstructural modification obtained. The vast buildup of the crystallites is attributed to the deposition rate, which is in agreement with the statement made from the study in Ref. [6] that increasing the concentrations of composite might propagate and lead to the increase in the deposition rate, hence making nucleation process precede the crystallites growing rate.

Since diffusion progress influences topography, it is essential to mention that the diffusion of ions from the deposition bath into the nucleus of the coating matrix is often gradual under the influence of the applied voltage/current density and increased electrodeposition time [1].

3.3 XRD/Raman analysis for deposited sample

Figure 9 shows XRD pattern of Zn−Al−7Sn−Ti−0.3V alloy. This implies that additive metal matrix of Al, Ti, and Sn composite particulates significantly

re-structure peak with dominate of crystal within the deposited system. The existing phases include $Zn_2Sn_2O_3$, $TiO_7{\cdot}Sn_2O_3$ and $Al_2O_3{\cdot}Zn_3O_{12}$ as shown in Fig. 9. The observed higher peak of the examined phases might be due to the induced metal matrix blended in the bath constituent which resulted in coherent structure and obviously led to formation of better intermetallic interface. It was reported that interaction between strengthening phases ultimately produces a crystal orientation of grain size rather than the chemical dissolution [7,20].

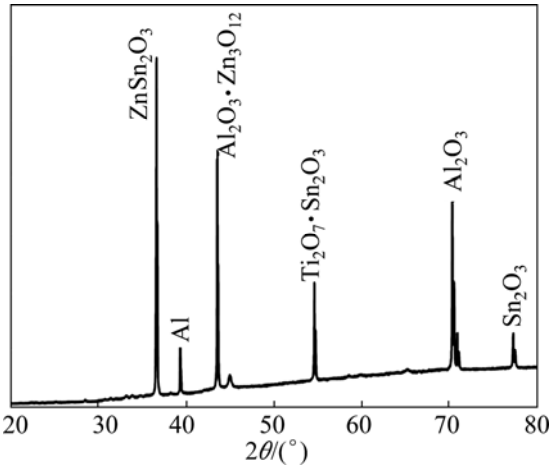

Fig. 9 XRD pattern of Zn−Al−13Sn− Ti−0.5V

Although nucleation is said to influence the nature of coating in codeposition system, inter-diffused and adsorbed composite particulates that are fused at the processed metal interface provide a nucleation site which enhanced zinc-rich composite nucleation matrix and crystal compartment. The EDS elemental observation and Raman depth in Fig. 10 have a subsequent correlation with the strengthening phases observed from the XRD pattern.

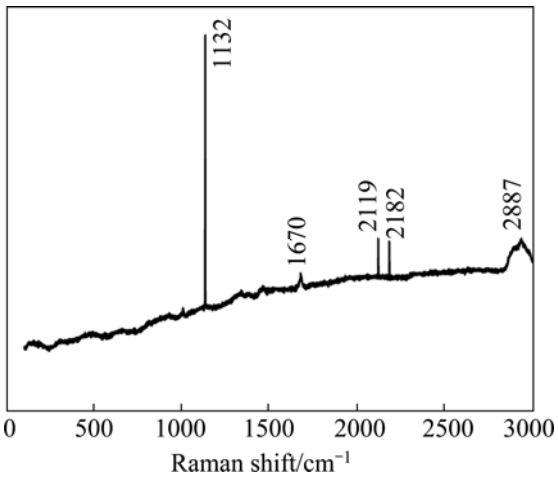

Fig. 10 Raman spectrum for Zn−Al−7Sn−Ti−0.3V chloride deposited sample

3.4 Microhardness studies

The average microhardness (HVN) values of the deposited coatings are summarized in Fig. 11. The hardness of as-received (Control) sample is HVN 33.4. The hardness profile data for all the deposited coatings show significant increase with HVN 299 for Zn−Al−7Sn−Ti−0.3V followed by HVN 248 for Zn−Al−13Sn−Ti−0.5V.

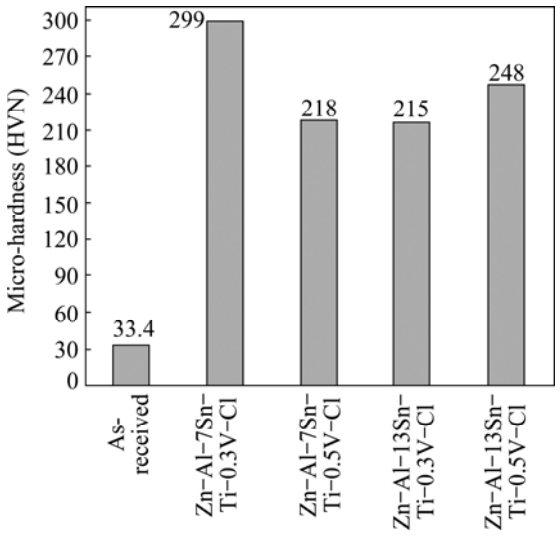

Fig. 11 Microhardness for Zn−Al−Sn−Ti chloride deposited sample

From all facts, the improvement in hardness obviously provides a geometric increase over the substrate and this is attributed to the crystal formation and superior nucleation. The adhesion and nucleation which yield the significant micro-hardness depend on the operating condition. Microstructural evolution in thin film coating is linked to processing parameters. This invariably results in the buildup of surface hardness improvement and is in agreement with the studies in Refs. [14,15, 23] .

3.5 Wear rate evaluation of deposited sample

Figure 12 shows variation of the wear rate as a function of time across the coating system and their deposited matrix. A remarkable improvement was obtained for all coated systems as a result of improved crystal and structural modification against the control sample. The wear loss is very high for the as-received sample with approximately 2.351 g/min. This is indeed expected due to the lack of surface protection.

Obviously, the condition for improved wear resistance was seen as a result of content of individual proportion of the metal solid grain. Composite coating is related to structure and chemical composition [6]. Composite−SnO_2−TiO_2 hence provides refinement in grain structure that provides resistance to dislocation trend of the interfacial matrix at the coating interface.

The wear scar morphology of the composite coating establishes the stability of the coatings on the substrate. Figures 13, 14 and 15 show the worn surface micrographs of samples. It can be seen from the scars that severe plastic deformation, massive grooves, and pits dominate the surface of the as-received substrate. On the other hand, the coated materials solid grain embedded were still visibly seen along the wear track interface.

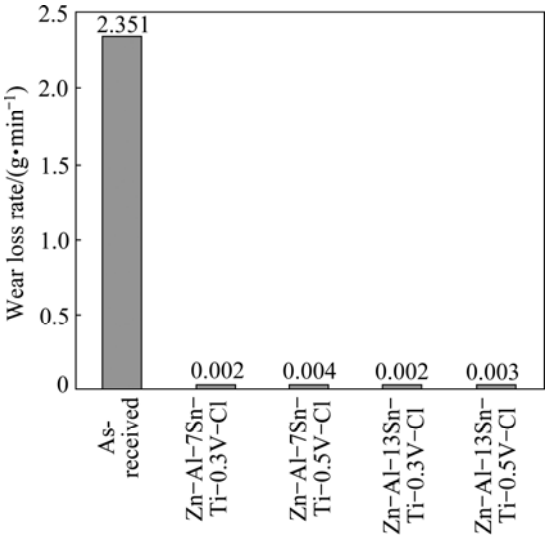

Fig. 12 Variation of wear loss rate with time for Zn−Al−Sn−Ti−Cl

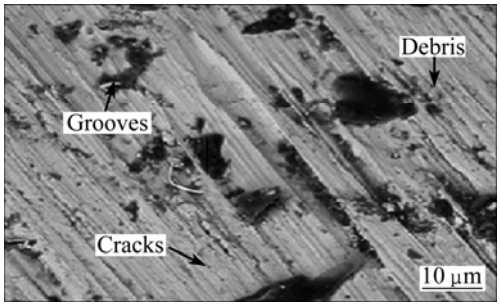

Fig. 13 SEM image of wear scar of as-received sample

With unseen pit formation and stress resistance crystal modification, it is quite advantageous for wear degradation of the quaternary alloy. Hence, strong adhesion of the processed fabricated coating that resists dislocation is justified by the induced film particulate. Subsequently, the EDX study of the wear scar shown in Fig. 14 indicates a possible elemental feature of the coating particulates with a proof of slight damage scar.

To further compare the wear structure and the degree of damage between the Zn−Al−7Sn−Ti−0.3V and Zn−Al−13Sn−Ti−0.5V from reciprocating sliding tester results, Fig. 15 shows the OPM micrographs which enable us to access the wear product at a lower magnification. Zn−Al−13Sn−Ti−0.5V has little debris

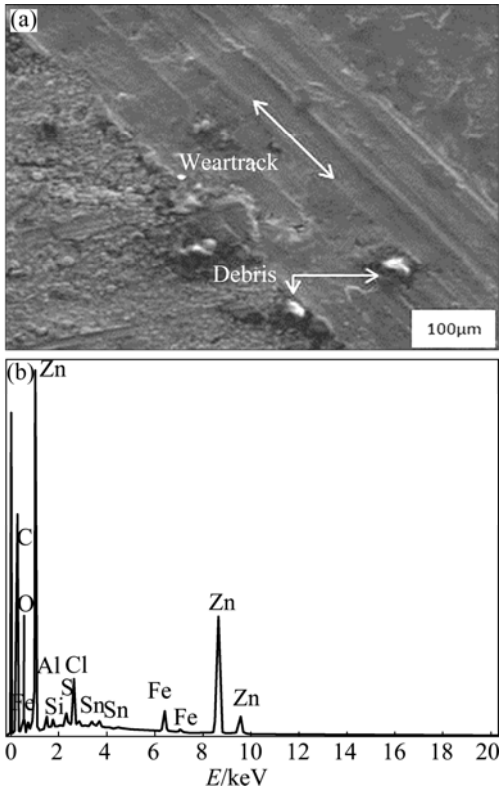

Fig. 14 SEM image (a) and EDS result (b) of wear track of Zn−Al− 7Sn−Ti−Cl−0.3V

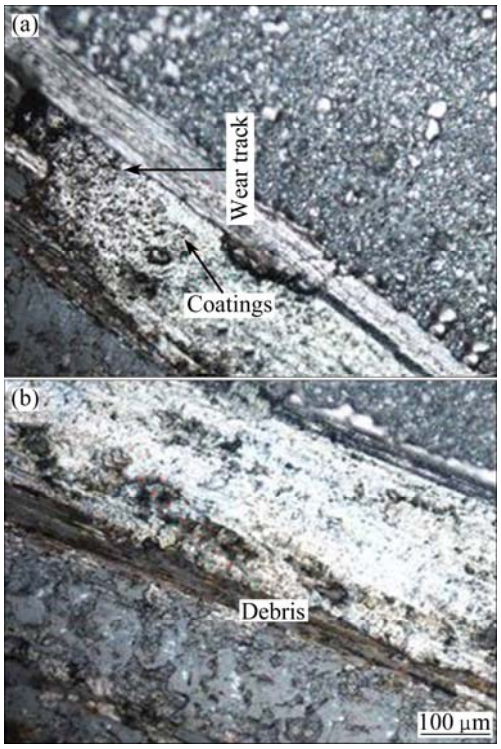

Fig. 15 OP micrographs of wear scars for Zn−Al−7Sn−Ti (a) and Zn−Al−13Sn−Ti (b) chloride deposited sample

around the edges while the formal refuse dislocation and hence pose rejection of debris along the wear track scars. It is worth noting that composite matrix is anti-oxidative

and abrasive in properties which provide resistance to certain deformation. Certain quantity of titanium oxide (TiO_2) and alumina (Al_2O_3) are found to prolong coating life span against wear and thermal influence [23,27] which is in line with our findings in this study.

Figures 16 and 17 respectively show the variation of friction coefficients μ with sliding time and velocity of the deposited Zn−Al−7Sn−Ti−0.3V alloy. It is essential, that process operating parameters in sliding wear conditions, such as load, sliding speed and temperature, have little or no effect on frictional characteristics [31]. However, incorporation of zinc-rich composite particulates led to the decrease in friction coefficient. Although, friction coefficient and linear wear were substantially reduced by micro-structurally modified ceramics and composite compared with monolithic alumina. The presence of admixed condition, metal grain and composite embedded in the zinc has major contribution for the advanced propagation of better friction attained against the massive mild steel transition. In general, metal composite−matrix interaction has been seen as a contributor for frictional resistance and reduced plastic deformation.

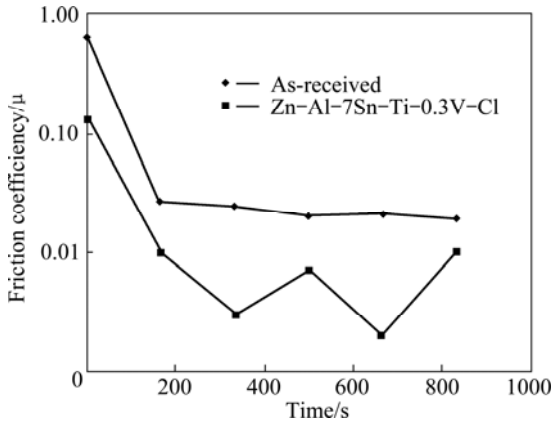

Fig. 16 Variation of wear friction coefficient against time for Zn−Al−7Sn−Ti−0.3V chloride deposited sample

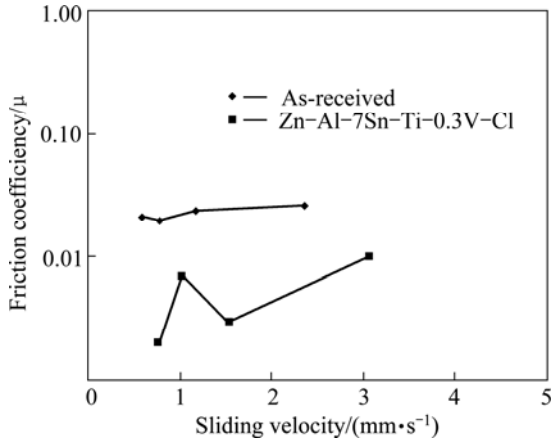

Fig. 17 Variation of wear friction coefficient against sliding velocity for Zn−Al−7Sn−Ti−0.3V chloride deposited sample

3.6 Electrochemical test result of composite coatings

Figure 18 shows the progression of deterioration and the susceptibility to corrode in 3.65% simulated medium with an induced current propagation examined by potential/current measurements. The differences in the potential values of the deposition were considered at 10 mA applied current. Obvious improvement in potential was discovered significantly for all coatings, which is due to the effects of coating film precipitated at the interface of the metal matrix. However, the substrate has less passive film formed on its surface, resulting in intensive corrosion attacked from the chloride solution with potential about −1.5 V which is more than double that of the deposited samples. The coating performance of all deposited alloys was high. Zn−Al−7Sn−Ti−0.3V alloy has the best performance among the series with higher potential and low corrosion rate. The summarized results of polarization measurements are also illustrated in Table 4, which are obtained from Tafel plots.

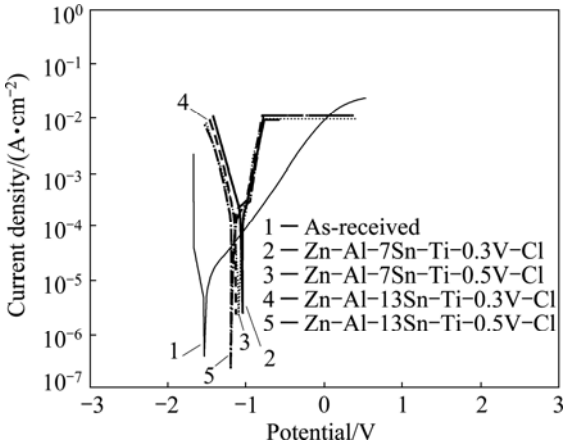

Fig. 18 Potentiodynamic polarization curves for Zn−Al−Sn−Ti chloride deposited

The corrosion current of as-received sample is 2.04 mA, the polarization resistance is 27.6 Ω and the high corrosion rate is about 4.1 mm/a which is expected due to the lack of any surface preservation as well as the exposure to chloride ion medium. The degradation was attributed to the high anodic potential, absorption of the halide ion on the oxide film which took place at the oxide solution interface and the formation of basic corrosion product oxide [12]. The corrosion current density J_{corr} of 2.71 μA was obtained for Zn−Al−7Sn−Ti−0.3V coating which is three order magnitude compared with the control sample. From the polarization resistance (R_p), R_p of deposited based coating is 1207.7 Ω, obviously it is the highest obtained from all the coated samples. The order of corrosion resistance is sample 2>3>4>5>1. The electro-oxidation stability of the deposited sample is traceable to the existence of the active electronegative phases and the strong independent

based active potential of the composite induced, which led to strengthening film within the interpose and hence retarded excessive deterioration.

The structural observations of the corrosion characteristics are seen for processed surface of Zn−Al−7Sn−Ti−0.3V−S and Zn−Al−13Sn−Ti−0.5V−S samples by AFM and OPM after corrosion test in 3.65% NaCl solution as illustrated in Figs. 19 and 20. The structure revealed few scales at interface. It is noteworthy to mention that the film scales are obviously in line with that reported in Ref. [1] during anodic dissolution, zinc-rich base formed excessive corrosion scale and hence posed metal matrix particulates on the surfaces. The penetration of ionic halide is not obviously potent and sufficient to accelerate dissolution of the composite through the coating boundaries and layer.

4 Conclusions

1) Deposition of the quaternary alloy from chloride bath is successful with bright, smooth and homogeneous deposits over the substrate.

2) The presence of composite induced in the bath fabricated coating gives a smaller grain size from SEM. The EDS, XRD spectra confirm the presence of composite inclusion at the interface.

3) The incorporation of the admixed composite provides a more stable and stress relieve coating compared with previous studies on zinc deposition. Co-deposition of Sn−Ti composite particles in zinc coating greatly improves the hardness. The microhardness of HVN 299 is attained for Zn−Al−7Sn−Ti−0.3V coating and HVN 248 for Zn−Al−13Sn−Ti−0.5V. This implies that coherent properties are obtained for all coatings with justifiable improvement against the approximately HVN 33.4 for the as-received substrate.

4) A highly improved corrosion resistance is obtained for co-deposited matrix with a positive and significant corrosion polarization.

Table 4 Summary of potentiodynamic polarization results

Sample	I_{corr}/A	J_{corr} /(A·cm^{-2})	R_P/Ω	φ_{corr}/V	Corrosion rate/ (mm·a^{-1})
As−received	2.04×10^{-3}	7.04×10^{-2}	27.60	−1.53900	4.100000
Zn−Al−7Sn−Ti−0.3V−Cl	2.19×10^{-6}	2.19×10^{-6}	1207.70	−1.05042	0.002509
Zn−Al−7Sn−Ti−0.5V−Cl	7.68×10^{-6}	7.68×10^{-6}	1026.10	−1.10443	0.003198
Zn−Al−13Sn−Ti−0.3V−Cl	1.58×10^{-5}	1.58×10^{-5}	758.43	−1.20178	0.003544
Zn−Al−13Sn−Ti−0.5V−Cl	5.37×10^{-5}	5.37×10^{-5}	269.55	−1.20239	0.005636

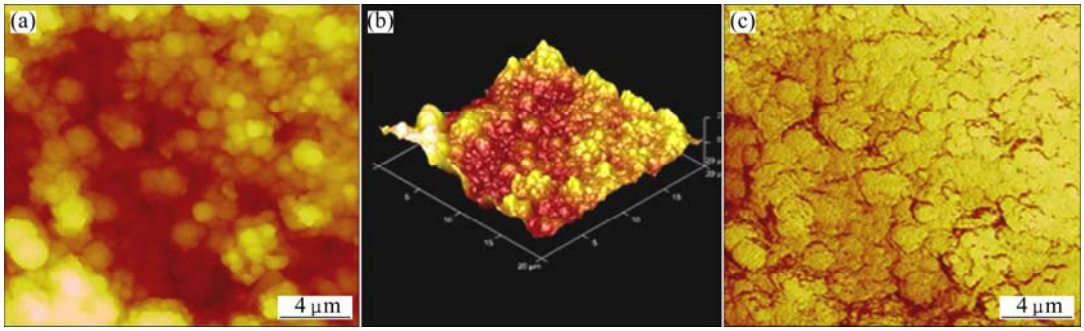

Fig. 19 AFM images of surface film obtained for Zn−Al−Sn−Ti−Cl−0.3V after corrosion: (a) 2D image; (b) 3D image; (c) Roughness analysis

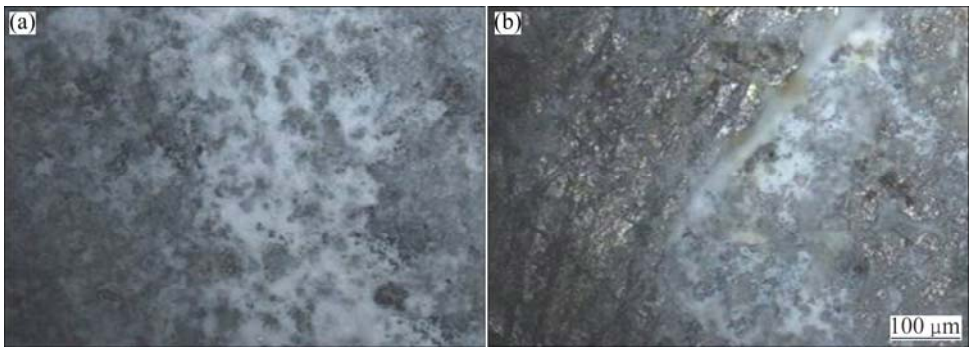

Fig. 20 Optical images of Zn−Al−Sn−Ti−Cl−0.3V (a) and Zn−Al−13Sn−Ti (b) chloride deposited samples after corrosion

5) The composite co-deposited coatings give a lower friction coefficient and reduce wear rate properties with the sliding friction and time.

Acknowledgements

The materials are based upon work supported financially by the National Research Foundation. The equipment was supported by Surface Engineering Research Centre (SERC), Tshwane University of Technology. Pretoria is deeply appreciated.

References

[1] PRAVEEN B M, VENKATESHA T V. Electrodeposition and properties of Zn-nanosized TiO_2 composite coatings [J]. Applied Surface Science, 2008, 254: 2418−2424.

[2] CHUEN C L, CHI M H. Zinc-nickel alloy coatings electrodeposition by pulse current and their corrosion behavior [J]. Journal of Coating Technology and Research, 2006, 3: 99−104.

[3] MOHANKUMAR C, PRAVEEN K, VENKATESHA V, VATHSALA K, NAYANA O. Electrodeposition and corrosion behavior of Zn−Ni and Zn−Ni−Fe_2O_3 coatings [J]. Journal of Coating Technology and Research, 2012, 9: 71−77.

[4] POPOOLA A P I, FAYOMI O S. Performance evaluation of zinc deposited mild steel in chloride medium [J]. International Journal of Electrochemical Science, 2011, 6: 3254−3254.

[5] ARICI M, NAZIR H, AKSU A. Investigation of Sn−Zn electrodeposition from acidic bath on EQCM [J]. Journal of Alloys and Compound, 2011, 509: 1534−1537.

[6] XU R, WANG J, GUO Z, WANG H. Effect of rare earth on microstructures and properties of Ni−W−P−CeO_2−SiO_2 nano-composite coating [J]. Journal of Rare Earth, 2008, 26: 579−583.

[7] FAYOMI O S I, POPOOLA A P I. Chemical interaction, interfacial effect and the microstructural characterization of the induced zinc–aluminum–solanum tuberosum in chloride solution on mild steel [J]. Research on Chemical Intermediate, 2013, 39: 6−15.

[8] YANG G, CHAI S, XIONG X, ZHANG S, YU L, ZHANG P. Preparations and tribological properties of surface modified Cu nanoparticles [J]. Transactions of Nonferrous Metals Society of China, 2012, 22: 366−372.

[9] SANCAKOGLU O, CULHA O, TOPARLI M, AGADAY B, CELIK E. Co-deposited Zn-submicron sized Al_2O_3 composite coatings: Production, characterization and micromechanical properties [J]. Journal of Material and Design, 2011, 32: 4054−4061.

[10] WANG T G, JEONG D, LIU Y, LYENGAR S, MELIN S, KIM K H. Study on nanocrystalline Cr_2O_3 films deposited by arc ion plating: II. Mechanical and tribological properties [J]. Journal of Surface Coating and Technology, 2012, 206: 2638−2644.

[11] HAMMAMI O, DHOUIBI L, BERCOT P, REZRAZI E M, TRIKI E. Study of Zn−Ni alloy coatings modified by nano-SiO_2 particles incorporation [J]. International Journal of Corrosion Science, 2012, 8: 1−8.

[12] POPOOLA A P I, FAYOMI O S I, POPOOLA O M. Electrochemical and mechanical properties of mild steel electroplated with Zn−Al [J]. International Journal of Electrochemical Science, 2012, 7: 4898−4917.

[13] ZHU X, CAI C, ZHENG G, ZHANG Z, LI J. Electrodeposition and corrosion behaviour of nanostructured Ni−TiN composite films [J]. Transactions of Nonferrous Metals Society of China, 2011, 21: 2216−2224.

[14] SHIBLI S M A, CHACKO F, DIVYA C. AL_2O_3−ZrO_2 mixed oxide composite incorporated aluminium rich zinc coatings for high wear resistance [J]. Journal of Corrosion Science, 2010, 52: 518−525.

[15] GOMES A, FRADE T, NOGUEIRA I D. Morphological characterization of Zn-based nanostructured thin films [J]. Current Microscopy Contributions to Advances in Science and Technology, 2012, 2: 1146−1153.

[16] FRADE T, BOUZON Z, GOMES A, da SILVA M I, PEREIRA M I. Pulsed-reverse current electrodeposition of Zn and Zn−TiO_2 nanocomposite films [J]. Surface and Coatings Technology, 2010, 204: 3592−3598.

[17] ZHANG W, LIU W, WANG C. Characterization and tribological investigation of sol-gel Al_2O_3 and doped Al_2O_3 films [J]. Journal of the European Ceramic Society, 2002, 22: 2869−2876.

[18] ABDEL A, BARAKAT M A, MOHAMED R M. Electrophered Zn−TiO_2−ZnO nanocomposite coating films for photocatalytic degration of 2-chlorophenol [J]. Applied Surface Science, 2008, 254: 4577−4583.

[19] YANG G, CHAI S, XIONG X, ZHANG S, YU L, ZHANG P. Preparations and tribological properties of surface modified Cu nanoparticles [J]. Transactions of Nonferrous Metals Society of China, 2012, 22(2): 366−372.

[20] FAYOMI O S I, ABDULWAHAB M, POPOOLA A P I. Properties evaluation of ternary surfactant-induced Zn−Ni−Al_2O_3 films on mild steel by electrolytic chemical deposition [J]. Journal of Ovonic Research, 2013, 9: 123−132.

[21] ABDEL A A, HASSAN H B, ABDEL RAHIM M A. Nanostructured Ni−P−TiO_2 composite coatings for electrocatalytic oxidation of small organic molecule [J]. Journal of Electroanalytical Chemistry, 2008, 620: 17−25.

[22] FUSTES J, GOMES A, SILVA D A, PEREIRA M I. Electrodeposition of Zn−TiO_2 nanocomposite films effect of bath composition [J]. Journal of Solid State Electrochemistry, 2008, 121: 1435−1443.

[23] POPOOLA A P I, FAYOMI O S I, POPOOLA O M. Comparative studies of microstructural, tribological and corrosion properties of plated Zn and Zn-alloy coatings [J]. International Journal of Electrochemical Science, 2012, 7: 4860−4870.

[24] SRIVASTAVA M, BALARAJU J N, RAVISHANKAR B, RAJAM K S. Improvement in the properties of nickel by nano-Cr_2O_3 incorporation [J]. Surface & Coatings Technology, 2010, 205: 66−75.

[25] DONG D, CHEN X H, XIAO W T, YANG G B, ZHANG P Y. Preparation and properties of electroless Ni−P−SiO_2 composite coatings [J]. Applied Surface Science, 2009, 255: 7051−7055.

[26] RAHMAN M J, SEN S R, MONIRUZZAMAN M, SHOROWORDI K M. Morphology and properties of electrodeposited Zn−Ni alloy coatings on mild steel [J]. Journal of Mechanical Engineering, 2009, 40: 9−12.

[27] KAZIMIEREZAK H, OZGA P. Electrodeposition of Sn−Zn and Sn−Zn−Mo layers from citrate solutions [J]. Surface Science, 2013, 607: 33−38.

[28] MO J L, ZHU M H, LEI B, LENG Y X, HUANG N. Comparison of tribological behavior of AlCrN and TiAlN coatings-deposition by physical vapor deposition [J]. Wear, 2007, 263: 1423−1429.

[29] SUBRAMANIAN B, MOHAN S, JAYAKRISHNAN S. Structural, microstructural and corrosion properties of brush plated copper−tin alloy coatings [J]. Surface and Coating Technology, 2006, 201: 1145−1151.

[30] ABOU-KRISHA M M, ASSAF F H, EL-NABY S A. Electrodeposition behavior of zinc-nickel-iron alloys from sulfate bath [J]. Journal of Coating Technology Research, 2009, 6: 391−399.

[31] ZUM GAHR K H. Modeling and microstructural modification of alumina ceramic for improved tribological properties [J]. Wear, 1996, 200: 215−224.

四元复合薄膜的形成特征、摩擦特性和耐腐蚀性能

Ojo Sunday Isaac FAYOMI, Abimbola Patricia Idowu POPOOLA

Department of Chemical, Metallurgical and Materials Engineering,
Tshwane University of Technology, P.M.B. X680, Pretoria, South Africa

摘　要：在工程应用中增强材料的腐蚀磨损性能是至关重要的。采用电沉积技术，研究从氯化物槽池中得到的 Zn−Al−SnO_2−TiO_2 (Zn−Al−Sn−Ti)复合薄膜的结构、电氧化性能。采用扫描电子显微镜联合能谱仪、光学显微镜和 X 射线衍射，研究薄膜的微观结构。采用动电位极化技术，研究在 3.65%NaCl 溶液中薄膜的电化学氧化和腐蚀行为，并采用原子力显微镜对其进行表征。采用高钻石硬扫描显微硬度测试仪和 CERT 往复滑动仪，研究电沉积薄膜的硬度和磨损行为。结构发现，成功获得了共沉积的复合材料和粒子，并得到了均匀、精细的嵌入颗粒结构以及改善的微观力学性能。所制备的四元薄膜的耐腐蚀性、硬度和稳定的耐磨性得到显著提高。

关键词：共沉积；显微组织演变；耐腐蚀性能；复合材料

(Edited by Xiang-qun LI)